Resolving the tensor structure of the Higgs coupling to Z bosons via Higgs-strahlung

Shankha Banerjee, Rick S. Gupta, Joey Y. Reiness, and Michael Spannowsky
Institute for Particle Physics Phenomenology, Durham University, South Road, Durham, DH1 3LE, United Kingdom

(Received 11 June 2019; published 3 December 2019)

We propose differential observables for $pp \to Z(\ell^+\ell^-)h(b\bar{b})$ that can be used to completely determine the tensor structure of the $hZZ^*/hZ\bar{f}f$ couplings relevant to this process in the dimension-six Standard Model (SM) effective field theory. In particular, we propose a strategy to probe the anomalous $hZ_{\mu\nu}Z^{\mu\nu}$ and $hZ_{\mu\nu}\tilde{Z}^{\mu\nu}$ vertices at the percent level. We show that this can be achieved by resurrecting the interference term between the transverse Zh amplitude, which receives contributions from the above couplings, and the dominant SM longitudinal amplitude. These contributions are hard to isolate without knowledge of the analytical amplitude, as they vanish unless the process is studied differentially in three different angular variables at the level of the Z-decay products. By also including the differential distributions with respect to energy variables, we obtain projected bounds for the two other tensor structures of the Higgs coupling to Z bosons.

DOI: 10.1103/PhysRevD.100.115004

I. INTRODUCTION

The discovery of the Higgs boson [1,2], the first electroweak-scale scalar particle, marked the starting point for an ongoing extensive program to study its interactions with particles of the Standard Model to high precision [3–5]. To perform this task, a theoretical framework was developed, compatible with high-scale UV completions of the Standard Model, which can mimic the kinematic impact of new resonances with masses beyond the energy reach of the LHC, i.e., the Standard Model effective field theory (SMEFT) framework [6–34]. Different bases were proposed to parametrize the SMEFT operators, e.g., the SILH [7] or Warsaw [8] bases, each providing a generic and rather model-independent way to probe the couplings of the Standard Model.

An important class of interactions to probe the electroweak sector is the couplings of the Higgs boson to gauge bosons, and in particular to the Z boson. There are 15 operators in the Warsaw basis at mass dimension six that contribute to the hZZ^* and $hZ\bar{f}f$ vertices (12 CP-even and 3 CP-odd operators). However, after electroweak symmetry breaking, these operators collectively only contribute to four interaction vertices for a given fermion, f. In the following section we explicitly show the relation between these dimension-six operators and the $hZZ^*/hZ\bar{f}f$ interaction vertices.

Relying exclusively on the process $pp \to Z(\ell^+\ell^-)h(b\bar{b})$, we propose to exploit differential distributions to constrain all four interaction vertices relevant to this process simultaneously. While there have been other studies devoted to this question [35,36], our approach is unique in that we systematically use our analytical knowledge of the squared amplitude to devise the experimental analysis strategy. For the squared amplitude at the level of the Z-decay products, the three possible helicities of the intermediate Z boson give rise to nine terms, each with a different angular dependence. These nine terms can be thought of as independent observables, each being sensitive to a different region of the final state's phase space. We assess which of these observables gets the dominant contribution from each of the four interaction vertices and thus devise a strategy to probe them simultaneously. In particular, we isolate the interference term between the longitudinal and transverse amplitudes that allows us to probe the $hZ_{\mu\nu}Z^{\mu\nu}$ and $hZ_{\mu\nu}\tilde{Z}^{\mu\nu}$ vertices in a clean and precise way.

This approach will be particularly useful for measurements during the upcoming high-luminosity runs of the LHC and at possible future high-energy colliders. It can be straightforwardly extended to other processes and different gauge bosons, and thus could play a crucial role in providing reliable and precise constraints in fits for effective operators. Exploiting and correlating different regions of phase space for individual processes can remove flat directions in the high-dimensional parameter space of effective theories.

II. DIFFERENTIAL ANATOMY OF $pp \to Z(\ell^+\ell^-)h(b\bar{b})$ IN THE SMEFT

Including all possible dimension-six corrections, the most general $hZZ^*/hZ\bar{f}f$ vertex can be parametrized as follows (see e.g., Refs. [12,37,38])[1]:

$$\Delta\mathcal{L}_6^{hZ\bar{f}f} \supset \delta\hat{g}^h_{ZZ}\frac{2m_Z^2}{v}h\frac{Z^\mu Z_\mu}{2} + \sum_f g^h_{Zf}\frac{h}{v}Z_\mu \bar{f}\gamma^\mu f + \kappa_{ZZ}\frac{h}{2v}Z^{\mu\nu}Z_{\mu\nu} + \tilde{\kappa}_{ZZ}\frac{h}{2v}Z^{\mu\nu}\tilde{Z}_{\mu\nu}. \quad (1)$$

For a single fermion generation, $f = u_L, d_L, u_R, d_R$ for corrections to the $pp \to Zh$ process and $f = e_L, e_R$ for corrections to the $e^+e^- \to Zh$ process. The only model-independent bound on the above couplings is an $\mathcal{O}(10\%)$ bound from the global Higgs coupling fit [3–5]. Translated to the above parametrization, this would constrain a linear combination of the above couplings including, the leptonic $hZ\bar{f}f$ contact terms. If we limit ourselves to only universal corrections, we must replace the second term above by $hZ_\mu\partial_\nu Z^{\mu\nu}$, which can be written as a linear combination of the contact terms using the equations of motion. The above parametrization is sufficient even if electroweak symmetry is nonlinearly realized (see e.g., [39]). For the case of linearly realized electroweak symmetry, these vertices arise in the unitary gauge upon electroweak symmetry breaking. In the Warsaw basis [8], we get the following contributions from the operators in Table I:

$$\begin{aligned}
\delta\hat{g}^h_{ZZ} &= \frac{v^2}{\Lambda^2}\left(c_{H\Box} + \frac{3c_{HD}}{4}\right),\\
g^h_{Zf} &= -\frac{2g}{c_{\theta_W}}\frac{v^2}{\Lambda^2}(|T_3^f|c^{(1)}_{HF} - T_3^f c^{(3)}_{HF} + (1/2 - |T_3^f|)c_{Hf}),\\
\kappa_{ZZ} &= \frac{2v^2}{\Lambda^2}(c^2_{\theta_W}c_{HW} + s^2_{\theta_W}c_{HB} + s_{\theta_W}c_{\theta_W}c_{HWB}),\\
\tilde{\kappa}_{ZZ} &= \frac{2v^2}{\Lambda^2}(c^2_{\theta_W}c_{H\tilde{W}} + s^2_{\theta_W}c_{H\tilde{B}} + s_{\theta_W}c_{\theta_W}c_{H\tilde{W}B}),
\end{aligned} \quad (2)$$

where $F = Q(L)$ if f is a quark (lepton).

If electroweak symmetry is linearly realized, there are additional constraints on the anomalous couplings in Eq. (1) because the same operators also contribute to different vertices already bounded by other measurements. Using the formalism of beyond-the-SM primaries [12], we obtain,

TABLE I. Dimension-six operators in the Warsaw basis that contribute to the anomalous $hZZ^*/hZ\bar{f}f$ couplings in Eq. (1). Here Q and L are the quark and lepton doublets. For other details regarding the notation see Ref. [8].

$\mathcal{O}_{H\Box} = (H^\dagger H)\Box(H^\dagger H)$	$\mathcal{O}^{(3)}_{HL} = iH^\dagger\sigma^a\overleftrightarrow{D}_\mu H\bar{L}\sigma^a\gamma^\mu L$
$\mathcal{O}_{HD} = (H^\dagger D_\mu H)^*(H^\dagger D_\mu H)$	$\mathcal{O}_{HB} = \lvert H\rvert^2 B_{\mu\nu}B^{\mu\nu}$
$\mathcal{O}_{Hu} = iH^\dagger\overleftrightarrow{D}_\mu H\bar{u}_R\gamma^\mu u_R$	$\mathcal{O}_{HWB} = H^\dagger\sigma^a H W^a_{\mu\nu}B^{\mu\nu}$
$\mathcal{O}_{Hd} = iH^\dagger\overleftrightarrow{D}_\mu H\bar{d}_R\gamma^\mu d_R$	$\mathcal{O}_{HW} = \lvert H\rvert^2 W_{\mu\nu}W^{\mu\nu}$
$\mathcal{O}_{He} = iH^\dagger\overleftrightarrow{D}_\mu H\bar{e}_R\gamma^\mu e_R$	$\mathcal{O}_{H\tilde{B}} = \lvert H\rvert^2 B_{\mu\nu}\tilde{B}^{\mu\nu}$
$\mathcal{O}^{(1)}_{HQ} = iH^\dagger\overleftrightarrow{D}_\mu H\bar{Q}\gamma^\mu Q$	$\mathcal{O}_{H\tilde{W}B} = H^\dagger\sigma^a H W^a_{\mu\nu}\tilde{B}^{\mu\nu}$
$\mathcal{O}^{(3)}_{HQ} = iH^\dagger\sigma^a\overleftrightarrow{D}_\mu H\bar{Q}\sigma^a\gamma^\mu Q$	$\mathcal{O}_{H\tilde{W}} = \lvert H\rvert^2 W^a_{\mu\nu}\tilde{W}^{a\mu\nu}$
$\mathcal{O}^{(1)}_{HL} = iH^\dagger\overleftrightarrow{D}_\mu H\bar{L}\gamma^\mu L$	

$$\begin{aligned}
\delta\hat{g}^h_{ZZ} &= \frac{2}{g^2}\left(\frac{\delta g^h_{VV}}{v} + s^2_{\theta_W}\delta g^Z_1 - t^2_{\theta_W}\delta\kappa_\gamma\right),\\
g^h_{Zf} &= \frac{2g}{c_{\theta_W}}Y_f t^2_{\theta_W}\delta\kappa_\gamma + 2\delta g^Z_f - \frac{2g}{c_{\theta_W}}(T_3^f c^2_{\theta_W} + Y_f s^2_{\theta_W})\delta g^Z_1,\\
\kappa_{ZZ} &= \frac{\delta\kappa_\gamma}{2c^2_{\theta_W}} + \kappa_{Z\gamma}\frac{c_{2\theta_W}}{2c^2_{\theta_W}} + \kappa_{\gamma\gamma},\\
\tilde{\kappa}_{ZZ} &= \frac{\delta\tilde{\kappa}_\gamma}{2c^2_{\theta_W}} + \tilde{\kappa}_{Z\gamma}\frac{c_{2\theta_W}}{2c^2_{\theta_W}} + \tilde{\kappa}_{\gamma\gamma}.
\end{aligned} \quad (3)$$

The couplings on the right-hand sides of the above equations are already constrained by LEP electroweak precision measurements or other Higgs measurements. The weakest constraint is on the triple gauge coupling $|\delta\kappa_\gamma| \lesssim 0.05$ [40], which appears on the right-hand sides of the first three equations above. This implies a 5%-level bound on all the CP-even Higgs anomalous couplings. Note that it is extremely important to measure the anomalous couplings on the left-hand sides of the above equations independently, despite these bounds. This is due to the fact that a verification of the above correlations can be used to test whether electroweak symmetry is linearly or nonlinearly realized.

The main objective of this work is to study the Higgs-strahlung process differentially with respect to energy and angular variables in order to individually constrain all the above anomalous couplings. To isolate the effects of the different couplings above it is most convenient to use the helicity amplitude formalism. At the $2 \to 2$ level, $f(\sigma)\bar{f}(-\sigma) \to Zh$, these helicity amplitudes are given by,

$$\begin{aligned}
\mathcal{M}^{\lambda=\pm}_\sigma &= \sigma\frac{1+\sigma\lambda\cos\Theta}{\sqrt{2}}\frac{gg^Z_f}{c_{\theta_W}}\frac{m_Z}{\sqrt{\hat{s}}}\left[1 + \left(\frac{g^h_{Zf}}{g^Z_f} + \kappa_{ZZ} - i\lambda\tilde{\kappa}_{ZZ}\right)\frac{\hat{s}}{2m_Z^2}\right],\\
\mathcal{M}^{\lambda=0}_\sigma &= -\sin\Theta\frac{gg^Z_f}{2c_{\theta_W}}\left[1 + \delta\hat{g}^h_{ZZ} + 2\kappa_{ZZ} + \frac{g^h_{Zf}}{g^Z_f}\left(-\frac{1}{2} + \frac{\hat{s}}{2m_Z^2}\right)\right],
\end{aligned} \quad (4)$$

[1]Note that in the parametrization of Refs. [31,38] both the custodial-preserving and -breaking hVV couplings contribute to $\delta\hat{g}^h_{ZZ}$.

where $\lambda = \pm 1$ and $\sigma = \pm 1$ are, respectively, the helicities of the Z boson and initial-state fermions, and $g_f^Z = g(T_3^f - Q_f s_{\theta_W}^2)/c_{\theta_W}$; $\sqrt{\hat{s}}$ is the partonic center-of-mass energy. We have kept only terms with the highest powers of $\gamma = \sqrt{\hat{s}}/(2m_Z)$ in the expressions above, both for the SM and EFT contributions. The neglected terms are smaller at least by a factor of $4m_Z^2/\hat{s}$. An exception is the next-to-leading EFT contribution for the $\lambda = 0$ mode, which we retain in order to keep the leading effect among the terms proportional to $\delta\hat{g}_{ZZ}^h$ term. For the full expressions see Ref. [41]. The above expressions assume that the quark moves in the positive z direction and the opposite case, where the antiquark direction coincides with the positive z direction, can be obtained by replacing $\sigma \to -\sigma$. Here and in what follows, unless explicitly mentioned, our analytical expressions hold for both quark and leptonic initial states.

At high energies the dominant EFT correction is to the longitudinal mode ($\lambda = 0$). For the $pp \to Zh$ process at the LHC, a linear combination of the four contact-term couplings, g_{Zf}^h, enters the EFT correction to the longitudinal cross section. This linear combination, given by,

$$g_{Z\mathbf{p}}^h = g_{Zu_L}^h - 0.76 g_{Zd_L}^h - 0.45 g_{Zu_R}^h + 0.14 g_{Zd_R}^h, \quad (5)$$

arises from the inability to disentangle the polarization of the initial partons, and that the luminosity ratio of up and down quarks remains roughly constant over the relevant energy range [31]. As shown in Ref. [31], by constraining these deviations that grow with energy, one can obtain strong per-mille-level bounds on $g_{Z\mathbf{p}}^h$, even with 300 fb^{-1} LHC data. The corrections to the longitudinal mode are also related to longitudinal double gauge-boson production due to the Goldstone boson equivalence theorem [42].

The unique signatures of the $\kappa_{ZZ}, \tilde{\kappa}_{ZZ}$ couplings arise from their contributions to the transverse Zh mode ($\lambda = \pm 1$), which in the SM is subdominant at high energies. The corrections to the transverse mode are hard to probe as this mode does not interfere with the dominant SM longitudinal mode. However, the longitudinal-transverse (LT) interference term is present at the level of the Z-decay products and vanishes only if we integrate inclusively over their phase space.[2] To recover this interference term and, in general, to maximally discriminate the transverse mode from the longitudinal mode, we must utilize the full dependence of the differential cross section on Θ, and the angular variables related to the Z-decay products (as defined in Fig. 1). Analytically, the amplitude can be most conveniently written in terms of $\hat{\varphi}$, the azimuthal angle of the positive-helicity lepton and $\hat{\theta}$, its polar angle in the Z rest frame. In terms of these variables the amplitude is given by,

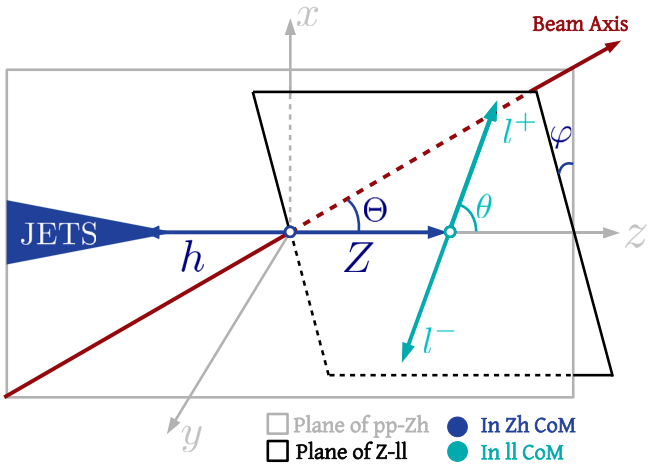

FIG. 1. Diagram showing the angles used to isolate the LT interference terms. Note that in fact two different frames of reference are represented: the c.m. frame of the Zh system (in which φ and Θ are defined) and the c.m. frame of the Z (in which θ is defined). We define the Cartesian axes $\{x, y, z\}$ the Zh center-of-mass frame, with z identified as the direction of the Z boson, y identified as the normal to the plane of the Z and beam axes, and finally x is defined such that it completes the right-handed set.

$$\mathcal{A}_h(\hat{s}, \Theta, \hat{\theta}, \hat{\varphi}) = \frac{-i\sqrt{2} g_\ell^Z}{\Gamma_Z} \sum_\lambda \mathcal{M}_\sigma^\lambda(\hat{s}, \Theta) d_{\lambda,1}^{J=1}(\hat{\theta}) e^{i\lambda\hat{\varphi}} \quad (6)$$

where $d_{\lambda,1}^{J=1}(\hat{\theta})$ are the Wigner functions (see e.g., Ref. [47]), Γ_Z is the Z width and $g_\ell^Z = g(T_3^\ell - Q_\ell s_{\theta_W}^2)/c_{\theta_W}$. Given that the polarization of the final-state lepton is not experimentally accessible, we express the squared amplitude (after summing over the final lepton polarizations) in terms of θ and φ, the analogous angles for the positively-charged lepton,

$$\sum_{L,R} |\mathcal{A}(\hat{s}, \Theta, \theta, \varphi)|^2 = \alpha_L |\mathcal{A}_h(\hat{s}, \Theta, \theta, \varphi)|^2 + \alpha_R |\mathcal{A}_h(\hat{s}, \Theta, \pi - \theta, \pi + \varphi)|^2, \quad (7)$$

where $\alpha_{L,R} = (g_{l_{L,R}}^Z)^2/[(g_{l_L}^Z)^2 + (g_{l_R}^Z)^2]$ is the fraction of $Z \to \ell^+\ell^-$ decays to leptons with left-handed (right-handed) chiralities. The above equation follows from the fact that for left-handed chiralities, the positive-helicity lepton is the positively charged lepton, whereas it is the negatively charged lepton for right-handed chiralities, so that for the latter case $(\hat{\theta}, \hat{\varphi}) = (\pi - \theta, \pi + \varphi)$. Using Eqs. (4), (6), and (7) one can write the full angular dependence of the squared amplitude, giving nine angular functions of Θ, θ and φ (see also Refs. [33,48,49]),

[2]This is analogous to the case of double gauge-boson production where a similar situation arises for certain triple gauge-boson deformations that contribute to helicity amplitudes that are subdominant in the SM [43–46].

$$\sum_{L,R}|\mathcal{A}(\hat{s},\Theta,\theta,\varphi)|^2$$
$$= a_{LL}\sin^2\Theta\sin^2\theta + a^1_{TT}\cos\Theta\cos\theta + a^2_{TT}(1+\cos^2\Theta)(1+\cos^2\theta) + \cos\varphi\sin\Theta\sin\theta \times (a^1_{LT} + a^2_{LT}\cos\theta\cos\Theta) + \sin\varphi\sin\Theta\sin\theta \times (\tilde{a}^1_{LT} + \tilde{a}^2_{LT}\cos\theta\cos\Theta) + a_{TT'}\cos 2\varphi\sin^2\Theta\sin^2\theta + \tilde{a}_{TT'}\sin 2\varphi\sin^2\Theta\sin^2\theta. \quad (8)$$

The subscripts of the above coefficients denote the Z polarization of the two interfering amplitudes, with TT' denoting the interference of two transverse amplitudes with opposite polarizations. These coefficients should be thought of as independently measurable observables.

Expressions for the nine coefficients above in terms of the anomalous couplings are given in Table II. The expressions in Table II utilize Eq. (4) which assumes that the initial quark direction coincides with the positive z direction. To obtain the final expressions relevant for the LHC we must average over this and the other possibility that the antiquark moves in the positive z direction [which is obtained by replacing $\sigma \to -\sigma$ in Eq. (4) and Table II]. This leads to vanishing a^1_{TT}, a^1_{LT} and $\tilde{a}^1_{LT}$ while keeping the other coefficients unchanged. Notice that powers of $\gamma = \sqrt{\hat{s}}/(2m_Z)$ lead to a parametric enhancement in some of the contributions to the coefficients. The dominant EFT contribution is that of g^h_{Zf} to a_{LL}. This coefficient also receives a subdominant contribution from $\delta\hat{g}^h_{ZZ}$. A linear combination of κ_{ZZ} and g^h_{Zf} gives the dominant contribution to three of the remaining coefficients, namely a^2_{TT}, a^2_{LT} and $a^1_{TT'}$. Similarly, $\tilde{\kappa}_{ZZ}$ is the only coupling that contributes to the two nonzero CP-violating parameters: $\tilde{a}^2_{LT}$ and $\tilde{a}_{TT'}$.

As anticipated, the parametrically largest contribution is to the LT interference terms,

$$\frac{a^2_{LT}}{4}\cos\varphi\sin 2\theta\sin 2\Theta + \frac{\tilde{a}^2_{LT}}{4}\sin\varphi\sin 2\theta\sin 2\Theta. \quad (9)$$

By looking at the dependence of a_{LL}, a^2_{LT} and $\tilde{a}^2_{LT}$ on the initial quark helicity, σ, we see that the linear combination of g^h_{Zf} couplings that enters a^2_{LT} and $\tilde{a}^2_{LT}$ for the $pp \to Zh$ process is again $g^h_{Z\mathbf{p}}$ defined in Eq. (5). Once $g^h_{Z\mathbf{p}}$ is very precisely constrained by constraining a_{LL} at high energies, one can separate the contribution of κ_{ZZ} to the two coefficients mentioned above. In the following sections we isolate these terms in our experimental analysis in order to constrain κ_{ZZ} and $\tilde{\kappa}_{ZZ}$. Notice that the above terms give no contribution if we integrate inclusively over either Θ, θ or φ. It is therefore highly nontrivial to access the LT interference term if one is not guided by the analytical form above.

Finally, we constrain $\delta\hat{g}^h_{ZZ}$. This coupling only rescales the SM hZZ coupling and hence all SM differential distributions. In order to constrain this coupling one needs to access its contribution to a_{LL}, which is subdominant in γ (see Table II). Ideally, one can perform a fit to the differential distribution with respect to $\hat{s}$ to extract both the dominant and subdominant pieces. In this work we will study the differential distribution with respect to $\hat{s}$ in two ranges, a low-energy and high-energy range, in order to individually constrain both g^h_{ZZ} and $g^h_{Z\mathbf{p}}$ (see Sec. III).

We have thus identified four observables to constrain the four anomalous couplings in Eq. (1): the differential $pp \to Zh$ cross section with respect to $\hat{s}$ at high and low energies, and the angular observables a^2_{LT} and $\tilde{a}^2_{LT}$. While we have chosen the observables that receive the largest EFT corrections parametrically, ideally one should use all the information contained in the nine coefficients in Eq. (8) (especially in the unsuppressed $a^2_{TT}, a_{TT'}$ and $\tilde{a}_{TT'}$) to obtain the strongest possible constraints on the Higgs anomalous couplings in Eq. (1). We leave this for future work.

We have so far considered only the effect of the anomalous Higgs couplings in Eq. (1). The $pp \to Z(\ell^+\ell^-)h(b\bar{b})$ process, however, also gets contributions [12] from operators that rescale the $hb\bar{b}$ and $Z\bar{f}f$ couplings (that we parametrize here by $\delta\hat{g}^h_{b\bar{b}}$ and $\delta\hat{g}^Z_f$ respectively) and from the vertices,

TABLE II. Contribution of the different anomalous couplings in Eq. (1) to the angular coefficients in Eq. (8) up to linear order. The above expressions hold for the case that the initial quark direction coincides with the positive z direction. To obtain the final expressions relevant for the LHC we must average over this and the other possibility that the antiquark moves in the positive z direction (which is obtained by replacing $\sigma \to -\sigma$). This leads to vanishing a^1_{TT}, a^1_{LT} and $\tilde{a}^1_{LT}$ while keeping the other coefficients unchanged. Contributions subdominant in $\gamma^{-1} = 2m_Z/\sqrt{s}$ have been neglected, with the exception of the next-to-leading EFT contribution to a_{LL}, which we retain in order to keep the leading effect of the $\delta\hat{g}^h_{ZZ}$ term. The terms neglected are smaller by at least a factor of $1/\gamma^2$. Here $\epsilon_{LR} = \alpha_L - \alpha_R, \mathcal{G} = g g^Z_f \sqrt{(g^Z_{l_L})^2 + (g^Z_{l_R})^2}/(c_{\theta_W}\Gamma_Z)$ and Γ_Z is the Z width. The SM part of our results is in complete agreement with Ref. [50].

a_{LL}	$\frac{\mathcal{G}^2}{4}[1 + 2\delta\hat{g}^h_{ZZ} + 4\kappa_{ZZ} + \frac{g^h_{Zf}}{g^Z_f}(-1+4\gamma^2)]$
a^1_{TT}	$\frac{\mathcal{G}^2\sigma\epsilon_{LR}}{2\gamma^2}[1 + 4(\frac{g^h_{Zf}}{g^Z_f} + \kappa_{ZZ})\gamma^2]$
a^2_{TT}	$\frac{\mathcal{G}^2}{8\gamma^2}[1 + 4(\frac{g^h_{Zf}}{g^Z_f} + \kappa_{ZZ})\gamma^2]$
a^1_{LT}	$-\frac{\mathcal{G}^2\sigma\epsilon_{LR}}{2\gamma}[1 + 2(\frac{2g^h_{Zf}}{g^Z_f} + \kappa_{ZZ})\gamma^2]$
a^2_{LT}	$-\frac{\mathcal{G}^2}{2\gamma}[1 + 2(\frac{2g^h_{Zf}}{g^Z_f} + \kappa_{ZZ})\gamma^2]$
$\tilde{a}^1_{LT}$	$-\mathcal{G}^2\sigma\epsilon_{LR}\tilde{\kappa}_{ZZ}\gamma$
$\tilde{a}^2_{LT}$	$-\mathcal{G}^2\tilde{\kappa}_{ZZ}\gamma$
$a_{TT'}$	$\frac{\mathcal{G}^2}{8\gamma^2}[1 + 4(\frac{g^h_{Zf}}{g^Z_f} + \kappa_{ZZ})\gamma^2]$
$\tilde{a}_{TT'}$	$\frac{\mathcal{G}^2}{2}\tilde{\kappa}_{ZZ}$

$$\kappa_{Z\gamma}\frac{h}{v}A^{\mu\nu}Z_{\mu\nu}+\tilde{\kappa}_{Z\gamma}\frac{h}{v}A^{\mu\nu}\tilde{Z}_{\mu\nu}. \tag{10}$$

The effect of these couplings can be incorporated by simply replacing in all our expressions,

$$\begin{aligned}\delta\hat{g}^h_{ZZ} &\to \delta\hat{g}^h_{ZZ}+\delta\hat{g}^h_{b\bar{b}}+\delta\hat{g}^Z_f,\\ \kappa_{ZZ} &\to \kappa_{ZZ}+\frac{Q_f e}{g^Z_f}\kappa_{Z\gamma},\\ \tilde{\kappa}_{ZZ} &\to \tilde{\kappa}_{ZZ}+\frac{Q_f e}{g^Z_f}\tilde{\kappa}_{Z\gamma},\end{aligned} \tag{11}$$

where for the last two replacements we have assumed $\hat{s}\gg m_Z^2$. At the $pp\to Zh$ level, the last two replacements become $\kappa_{ZZ}\to\kappa_{ZZ}+0.3\kappa_{Z\gamma}$, $\tilde{\kappa}_{ZZ}\to\tilde{\kappa}_{ZZ}+0.3\tilde{\kappa}_{Z\gamma}$. These degeneracies can be resolved straightforwardly by including LEP Z-pole data and information from other Higgs-production and decay channels.

III. ANALYSIS AND RESULTS

The following analysis is performed for $\sqrt{s}=14$ TeV. We base our analysis strategy on the one described in Ref. [31]. Our signal is comprised of $Zh\to\ell^+\ell^- b\bar{b}$ production from a pair of quarks and gluons with the former being the dominant contribution. We consider the dominant backgrounds, which consist of the SM Zh production decaying in the same final state, $Zb\bar{b}$ (where the subdominant gluon-initiated case is also taken into account) and $Z+$ jets (where jets include c quarks as well, but they are not explicitly tagged), where the light jets can fake as b-tagged jets. We also consider the leptonic mode of the $t\bar{t}$ process.

In order to isolate events where a boosted Higgs boson gives rise to the $b\bar{b}$ pair, from significantly larger QCD backgrounds, we resort to a fat jet analysis instead of a resolved analysis. For the fat jet analysis, we follow the BDRS technique [51–53] with small alterations in order to maximize the sensitivity. The details of the analysis are presented in the Appendix. Using a multivariate analysis (MVA), described in detail in the Appendix, we enhance the ratio of SM $Zh(b\bar{b})$ to $Zb\bar{b}$ events from a factor of 0.02 to about 0.2, still keeping around 500 $Zh(b\bar{b})$ events with 3 ab^{-1} data for a certain value of the MVA score. For a tighter MVA cut, we increase this ratio even further (to about ∼0.5). We will use both of these cuts in what follows.

We now use the four differential observables identified in Sec. II to obtain sensitivity projections for the four anomalous couplings in Eq. (1). We will determine the value of a given anomalous coupling that can be excluded at the 68% C.L. level, assuming that the observed number of events agrees with the SM. For a given value of the anomalous couplings, one can estimate the cutoff for our EFT by putting the Wilson coefficients, $c_i=1$, into Eq. (2). We will ignore in our analysis any event with a Zh invariant mass, M_{Zh}, larger than the estimated cutoff.

(a) *High-energy M_{Zh} distribution:* As already discussed, by just looking at the tail of the distribution with respect to M_{Zh}, one can constrain the leading energy enhanced contribution to a_{LL} induced by $g^h_{Z\mathbf{p}}$. The analysis in Ref. [31] revealed that one can obtain the following per-mille-level bound with 3 ab^{-1} data:

$$|g^h_{Z\mathbf{p}}|<5\times10^{-4}. \tag{12}$$

(b) *Low-energy M_{Zh} distribution:* Once the M_{Zh} distribution at high energies has been used to obtain the strong bound on $g^h_{Z\mathbf{p}}$ in Eq. (12), one can use the lower-energy bins to constrain the subdominant contribution of $\delta\hat{g}^h_{ZZ}$ (see Table II). We have checked, for instance, that for $M_{Zh}<950$ GeV, values of $g^h_{Z\mathbf{p}}$ smaller than the bound in Eq. (12) have a negligible contribution. Using the sample with the tighter MVA cut, we distribute the data into 100 GeV M_{Zh} bins. We then construct a bin-by-bin χ^2 function, where for each bin we add in quadrature a 5% systematic error to the statistical error. Energy-independent corrections from κ_{ZZ} to a^2_{TT} (see Table II) are also of the same order as the $\delta\hat{g}^h_{ZZ}$ contribution. Including these corrections, for an integrated luminosity of 3 ab^{-1}, we finally obtain a bound on the linear combination,

$$-0.06<\delta\hat{g}^h_{ZZ}+3.5\kappa_{ZZ}<0.07, \tag{13}$$

where we have ignored any events with $M_{Zh}>950$ GeV, the EFT cutoff estimated as discussed above. The precise linear combination that appears above is of course dependent on the choice of our cuts and has been obtained numerically after our collider analysis.

(c) *The LT interference terms a^2_{LT} and $\tilde{a}^2_{LT}$:* We want to isolate the terms in Eq. (9), which vanish upon an inclusive integration over either Θ, θ and φ. To visually show the impact of turning on the couplings κ_{ZZ} and $\tilde{\kappa}_{ZZ}$, we carry out a weighted integration, which gives an event a weight equal to the sign of $\sin2\Theta\sin2\theta$. This yields an asymmetry variable, $\xi(\varphi)$, which is expected to have a $\cos\varphi$ ($\sin\varphi$) dependence for the κ_{ZZ} ($\tilde{\kappa}_{ZZ}$) contribution. We show a normalized histogram for ξ with respect to φ in Fig. 2. As expected from Table II, we also find an SM contribution to a^2_{LT} with respect to which the EFT contribution grows as $2\kappa_{ZZ}\gamma^2$ at high energies. The contribution of the remaining background to a^2_{LT} is about 4 times the SM contribution.

For the final extraction of a^2_{LT} and $\tilde{a}^2_{LT}$ we convolute the observed angular distribution in each energy bin with the weight functions $\cos\varphi\sin2\theta\sin2\Theta$ and $\sin\varphi\sin2\theta\sin2\Theta$ respectively. It can be checked that this uniquely isolates a^2_{LT} and $\tilde{a}^2_{LT}$ respectively among the nine

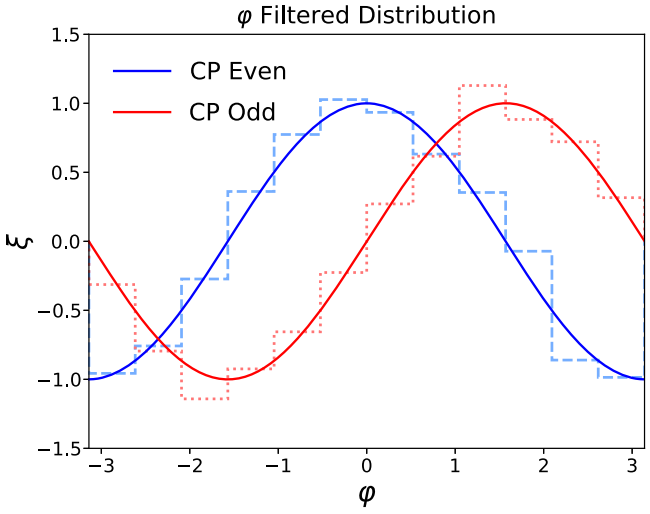

FIG. 2. We show here the LT interference terms in Eq. (9) for CP-odd and -even (from the couplings κ_{ZZ} and $\tilde{\kappa}_{ZZ}$) EFT contributions. To visualize these contributions we have carried out a weighted integration giving a negative weight whenever the product $\sin 2\Theta \sin 2\theta$ is negative. This yields the asymmetry variable, $\xi(\varphi)$, with the expected $\cos\varphi$ ($\sin\varphi$) dependence for the κ_{ZZ} ($\tilde{\kappa}_{ZZ}$) contribution shown above.

coefficients of Eq. (8). Using the fact that these coefficients depend linearly on κ_{ZZ} and $\tilde{\kappa}_{ZZ}$ (assuming again that $g^h_{Z\mathbf{p}}$ is precisely constrained), respectively, we translate the values of the coefficients to these anomalous couplings. In practice to carry out the above convolution we perform a weighted sum over the simulated Monte Carlo events with the above weights where we use the sample with the looser MVA cut. To estimate the uncertainties we split out Monte Carlo sample into multiple smaller samples each with the expected number of events at 3 ab^{-1} and find the values of κ_{ZZ} and $\tilde{\kappa}_{ZZ}$ in each case. We finally obtain the 1σ bound:

$$-0.07 < \kappa_{ZZ} < 0.07, \qquad -0.07 < \tilde{\kappa}_{ZZ} < 0.07. \tag{14}$$

Again we ignore events with M_{Zh} larger than the cutoff estimated by the procedure discussed above. In any case our result is not too dependent on this procedure as we obtain maximal sensitivity from events in the $450 \lesssim M_{Zh} \lesssim 850$ GeV range, which is safely below the estimated cutoff.

We now compare our final bounds in Eq. (14) with other existing projections on the measurement of κ_{ZZ} and $\tilde{\kappa}_{ZZ}$. The projections of Ref. [54] from the $h \to ZZ \to 4l$ process at 3 ab^{-1} using the matrix element method are $|\kappa_{ZZ}| < 0.04$ and $|\tilde{\kappa}_{ZZ}| < 0.09$.[3] Bounds on κ_{ZZ} can also be obtained using Eq. (3) and the 3 ab^{-1} projection from diboson production $\delta\kappa_\gamma \lesssim 0.01$ [55]. While this results in the more stringent bound $\kappa_{ZZ} \lesssim 0.01$, it assumes that electroweak symmetry is linearly realized. If, instead, we want to establish (or disprove) that electroweak symmetry is linearly realized using precision Higgs physics, it is essential to measure all the couplings in Eq. (3) independently.

[3]The projections in Refs. [36,54] from $pp \to Zh$ are unfortunately not comparable to ours as these studies included high-energy regions of the phase space where the EFT rate is many times that of the SM. These results are thus not compatible with our assumption of $\mathcal{O}(1)$ Wilson coefficients.

IV. CONCLUSION

As we enter the era of higher energies and luminosities, the time has come to shift from using only rate information to performing differential studies that utilize more sophisticated kinematical observables. In this work we have shown how a differential study of the $pp \to Z(\ell^+\ell^-)h(b\bar{b})$ process can completely resolve the tensor structure of the $hZZ^*/hZ\bar{f}f$ contributions in the dimension-six SMEFT [see Eqs. (1) and (2)].

To achieve this, we have analytically studied the full differential cross section in the SMEFT [see Eq. (8)]. This has enabled us to identify differential observables that get leading contributions from the different anomalous vertices. Of the four possible anomalous Higgs couplings relevant to this process, $g^h_{Z\mathbf{p}}$ and $\delta\hat{g}^h_{ZZ}$ can be constrained using the differential distribution with respect to the Zh invariant mass. The leading contributions from κ_{ZZ} and $\tilde{\kappa}_{ZZ}$ are much more elusive. This is because the above couplings give corrections only to transverse Zh production, which does not interfere with the dominant SM amplitude for the longitudinal mode. The interference term [see Eq. (9)] can be recovered at the level of the Z-decay products but only if we perform the analysis differentially in three angular variables. We ultimately showed that at the high-luminosity LHC one can constrain $g^h_{Z\mathbf{p}}$ at the per-mille-level, $\delta\hat{g}^h_{ZZ}$ at the 5% level and the couplings κ_{ZZ} and $\tilde{\kappa}_{ZZ}$ at the percent level [see Eqs. (12), (13), and (14), respectively].

In this study we have identified four optimal observables in order to obtain simultaneous bounds on the four anomalous Higgs couplings. Our sensitivity estimates are thus conservative, as there are many more observables that we have not considered. Even for the observables we considered, our analysis did not utilize the full angular shape information. There is thus the possibility that significantly stronger bounds can be obtained if the full differential information contained in the matrix element squared (see Table II) is extracted by using, for example, the method of angular moments (see e.g., Refs. [56–58]) or advanced machine-learning tools. The approach advocated here is equally applicable to future leptonic colliders where it can be of even greater importance as, in this case, Higgs-strahlung is among the dominant Higgs production modes.

ACKNOWLEDGMENTS

We thank Amol Dighe and Shilpi Jain for helpful discussions. S. B. is supported by a Durham Junior Research

Fellowship COFUNDed by Durham University and the European Union, under grant agreement No. 609412.

APPENDIX: DETAILS OF THE COLLIDER ANALYSIS

Our analysis setup can be described in the following steps. We create our model containing all the effective vertices using FeynRules [59] and obtain the UFO [60] model implementation which is then fed into the MG5_aMC@NLO [61] package used to generate all the signal and background samples at leading order (LO). For the loop-induced processes, we perform the decays using MadSpin [62,63]. Next we hadronize and shower the events using the Pythia 8 [64,65] framework. Finally, we perform a simplified detector simulation, which we discuss shortly.

Since we are looking into a boosted topology, we generate the Zh and $Zb\bar{b}$ samples with the following generation-level cuts: $p_{T,(j,b)} > 15$ GeV, $p_{T,\ell} > 5$ GeV, $|y_j| < 4$, $|y_{b/\ell}| < 3$, $\Delta R_{b\bar{b}/bj/bl} > 0.2$, $\Delta R_{\ell^+\ell^-} > 0.15$, 70 GeV $< m_{\ell\ell} <$ 110 GeV, 75 GeV $< m_{b\bar{b}} <$ 155 GeV and $p_{T,\ell^+\ell^-} > 150$ GeV. Moreover, these processes are generated with an additional parton upon using the matrix element (ME) parton shower merging in the MLM merging scheme [66]. The events in the $Z+$jets channel are generated without the cut on the invariant mass of the jets and upon merging with up to three ME partons. All our event generations are at LO. Hence, in order to taken into account higher-order QCD corrections, we use next-to-leading-order (NLO) K factors. For the qq-initiated Zh samples, we include a bin-by-bin NLO corrected K factor in the reconstructed M_{Zh} (invariant mass of the double b-tagged filtered fat jet and the two isolated leptons) distribution for both the SM and the EFT signal [67]. For the gg-initiated counterpart, we multiply the LO cross section by a flat K factor of 2 [68]. For the tree-level $Zb\bar{b}$ and $Z+$jets backgrounds, we respectively use K factors of 1.4 (computed in the MG5_aMC@NLO framework) and 0.91 [69]. Finally, we consider an NLO correction of 1.8 [70] for the gg-initiated $Zb\bar{b}$ process. Further electroweak backgrounds [71] are found to be small.

As mentioned above, we use the BDRS technique to optimize our signal yield. The BDRS technique reconstructs jets upon using the Cambridge-Aachen (CA) algorithm [72,73] with a large cone radius in order to contain all the decay products ensuing from the relevant resonance. One then looks at the substructure of this fat jet by working backwards through the jet clustering. The algorithm requires us to stop when a substantial *mass drop*, $m_{j_1} < \mu m_j$ with $\mu = 0.66$, (where m_j is the mass of the fat jet) occurs for a reasonably symmetric splitting,

$$\frac{\min(p_{T,j_1}^2, p_{T,j_2}^2)}{m_j^2}\Delta R_{j_1,j_2}^2 > y_{\rm cut},$$

with $y_{\rm cut} = 0.09$. If the aforementioned criteria is not met, one removes the softer subjet, j_2 and j_1 is subjected to the above criteria. This iterative algorithm stops once one finally obtains two subjets, j_1 and j_2 which satisfy the mass drop criteria. In order to improve the reconstruction, the mass drop criteria is combined with the *filtering* algorithm. For this step, the two subjets j_1 and j_2 are further combined using the CA algorithm upon using a cone radius of $R_{\rm filt} = \min(0.3, R_{b\bar{b}}/2)$. Finally, only the hardest three filtered subjets are considered to reconstruct the resonance. However, in our study we find that using $R_{\rm filt} = \max(0.2, R_{b\bar{b}}/2)$ acts as a better choice in reducing backgrounds. Finally, we required the hardest two subjets to be b tagged with a tagging efficiency of 70%. The mistag rate of the light jets faking as b jets is taken to be a flat 2%.

Having witnessed the prowess of an MVA in Ref. [31], we refrain from doing the cut-based analysis (CBA) in this work.[4] First we construct fat jets with a cone radius of $R = 1.2$, $p_T > 80$ GeV and $|y| < 2.5$ in the FastJet [74] framework. Furthermore, we isolate the leptons with $p_T >$ 20 GeV and $|y| < 2.5$ ($e\mu$) upon requiring that the total hadronic activity around a cone of radius $R = 0.3$ about the lepton should be less than 10% of its p_T. We select events with exactly to oppositely charged same flavour isolated leptons. Before performing the MVA, we select the final state with loose cuts on several variables, *viz.*, 70 GeV $< m_{\ell^+\ell^-} <$ 110 GeV, $p_{T,\ell^+\ell^-} > 160$ GeV, $\Delta R_{\ell^+\ell^-} > 0.2$, $p_{T,\rm fatjet} > 60$ GeV, 95 GeV $< m_h <$ 155 GeV, $\Delta R_{b_i,\ell_j} >$ 0.4 and $\not{E}_T < 30$ GeV. The $\not{E}_T < 30$ GeV cut is imposed to almost completely remove the $t\bar{t}$ background. We also require that there is at least one fat jet associated with at least two B-meson tracks with $p_T > 15$ GeV. Furthermore, we require this fat jet to be double b tagged. The $Z+$jets, $gg \to Zh$, $t\bar{t}$ and $gg \to ZZ$ backgrounds being considerably subleading, the training of the boosted decision trees is performed only with the SM $q\bar{q} \to Zh$ and $Zb\bar{b}$ samples upon using the following variables, viz., $p_T(\ell_1, \ell_2)$, $\Delta R(b_i\ell_j/\ell_1\ell_2/b_1b_2)$, where i, $j = 1$, 2 and b_i, b_j are the b-tagged subjets inside the fat jet, m_Z, $p_T(Z)$, $\Delta\phi(J, Z)$, $\not{E}_T$, m_J, $p_T(J)$, $p_T(b_1, b_2)$, $p_T(b_1)/p_T(b_2)$, $|y(J)|$, where J is the reconstructed double b-tagged fat jet and Z is the reconstructed Z boson from the two isolated leptons. Our final variables of interest being the invariant mass of the reconstructed Zh system and the three angles mentioned below, we do not consider these variables while training our samples. We utilize the TMVA [75] framework to train the signal and background samples and ensure that there is no overtraining [76].

[4]Details of the CBA can be found in Ref. [31].

[1] G. Aad *et al.* (ATLAS Collaboration), Phys. Lett. B **716**, 1 (2012).
[2] S. Chatrchyan *et al.* (CMS Collaboration), Phys. Lett. B **716**, 30 (2012).
[3] G. Aad *et al.* (ATLAS, CMS Collaborations), J. High Energy Phys. 08 (2016) 045.
[4] Combined measurements of Higgs boson production and decay using up to 80 fb^{-1} of proton–proton collision data at $\sqrt{s} = 13$ TeV collected with the ATLAS experiment, Technical Report No. ATLAS-CONF-2018-031, CERN, Geneva, 2018.
[5] A. M. Sirunyan *et al.* (CMS Collaboration), Eur. Phys. J. C **79**, 421 (2019).
[6] W. Buchmuller and D. Wyler, Nucl. Phys. **B268**, 621 (1986).
[7] G. F. Giudice, C. Grojean, A. Pomarol, and R. Rattazzi, J. High Energy Phys. 06 (2007) 045.
[8] B. Grzadkowski, M. Iskrzynski, M. Misiak, and J. Rosiek, J. High Energy Phys. 10 (2010) 085.
[9] S. Banerjee, S. Mukhopadhyay, and B. Mukhopadhyaya, Phys. Rev. D **89**, 053010 (2014).
[10] J. Elias-Miró, C. Grojean, R. S. Gupta, and D. Marzocca, J. High Energy Phys. 05 (2014) 019.
[11] R. Contino, M. Ghezzi, C. Grojean, M. Muhlleitner, and M. Spira, J. High Energy Phys. 07 (2013) 035.
[12] R. S. Gupta, A. Pomarol, and F. Riva, Phys. Rev. D **91**, 035001 (2015).
[13] G. Amar, S. Banerjee, S. von Buddenbrock, A. S. Cornell, T. Mandal, B. Mellado, and B. Mukhopadhyaya, J. High Energy Phys. 02 (2015) 128.
[14] M. Buschmann, D. Goncalves, S. Kuttimalai, M. Schonherr, F. Krauss, and T. Plehn, J. High Energy Phys. 02 (2015) 038.
[15] N. Craig, M. Farina, M. McCullough, and M. Perelstein, J. High Energy Phys. 03 (2015) 146.
[16] J. Ellis, V. Sanz, and T. You, J. High Energy Phys. 07 (2014) 036.
[17] J. Ellis, V. Sanz, and T. You, J. High Energy Phys. 03 (2015) 157.
[18] S. Banerjee, T. Mandal, B. Mellado, and B. Mukhopadhyaya, J. High Energy Phys. 09 (2015) 057.
[19] C. Englert, R. Kogler, H. Schulz, and M. Spannowsky, Eur. Phys. J. C **76**, 393 (2016).
[20] J. Cohen, S. Bar-Shalom, and G. Eilam, Phys. Rev. D **94**, 035030 (2016).
[21] S.-F. Ge, H.-J. He, and R.-Q. Xiao, J. High Energy Phys. 10 (2016) 007.
[22] R. Contino, A. Falkowski, F. Goertz, C. Grojean, and F. Riva, J. High Energy Phys. 07 (2016) 144.
[23] A. Biekötter, J. Brehmer, and T. Plehn, Phys. Rev. D **94**, 055032 (2016).
[24] J. de Blas, M. Ciuchini, E. Franco, S. Mishima, M. Pierini, L. Reina, and L. Silvestrini, J. High Energy Phys. 12 (2016) 135.
[25] H. Denizli and A. Senol, Adv. High Energy Phys. **2018**, 1 (2018).
[26] T. Barklow, K. Fujii, S. Jung, R. Karl, J. List, T. Ogawa, M. E. Peskin, and J. Tian, Phys. Rev. D **97**, 053003 (2018).
[27] I. Brivio and M. Trott, Phys. Rep. **793**, 1 (2019).
[28] T. Barklow, K. Fujii, S. Jung, M. E. Peskin, and J. Tian, Phys. Rev. D **97**, 053004 (2018).
[29] H. Khanpour and M. Mohammadi Najafabadi, Phys. Rev. D **95**, 055026 (2017).
[30] C. Englert, R. Kogler, H. Schulz, and M. Spannowsky, Eur. Phys. J. C **77**, 789 (2017).
[31] S. Banerjee, C. Englert, R. S. Gupta, and M. Spannowsky, Phys. Rev. D **98**, 095012 (2018).
[32] A. Biekötter, T. Corbett, and T. Plehn, SciPost Phys. **6**, 064 (2019).
[33] D. Goncalves and J. Nakamura, Phys. Rev. D **99**, 055021 (2019).
[34] F. F. Freitas, C. K. Khosa, and V. Sanz, Phys. Rev. D **100**, 035040 (2019).
[35] R. Godbole, D. J. Miller, K. Mohan, and C. D. White, Phys. Lett. B **730**, 275 (2014).
[36] R. M. Godbole, D. J. Miller, K. A. Mohan, and C. D. White, J. High Energy Phys. 04 (2015) 103.
[37] G. Isidori, A. V. Manohar, and M. Trott, Phys. Lett. B **728**, 131 (2014).
[38] A. Pomarol, in *Proceedings, 2014 European School of High-Energy Physics (ESHEP 2014): Garderen, The Netherlands, 2014* (CERN, Geneva, 2016), pp. 59–77, arXiv:1412.4410.
[39] G. Isidori and M. Trott, J. High Energy Phys. 02 (2014) 082.
[40] A Combination of Preliminary Results on Gauge Boson Couplings Measured by the LEP experiments, Technical Reports No. LEPEWWG-TGC-2003-01, No. DELPHI-2003-068-PHYS-936, No. L3-Note-2826, No. LEP-EWWG-2006-01, No. OPAL-TN-739, No. ALEPH-2006-016-CONF-2003-012, CERN, Geneva, 2003, 2003 Summer Conferences.
[41] J. Nakamura, J. High Energy Phys. 08 (2017) 008.
[42] R. Franceschini, G. Panico, A. Pomarol, F. Riva, and A. Wulzer, J. High Energy Phys. 02 (2018) 111.
[43] K. Hagiwara, R. D. Peccei, D. Zeppenfeld, and K. Hikasa, Nucl. Phys. **B282**, 253 (1987).
[44] A. Azatov, R. Contino, C. S. Machado, and F. Riva, Phys. Rev. D **95**, 065014 (2017).
[45] G. Panico, F. Riva, and A. Wulzer, Phys. Lett. B **776**, 473 (2018).
[46] A. Azatov, J. Elias-Miro, Y. Reyimuaji, and E. Venturini, J. High Energy Phys. 10 (2017) 027.
[47] G. Panico, F. Riva, and A. Wulzer, Phys. Lett. B **776**, 473 (2018).
[48] J. C. Collins and D. E. Soper, Phys. Rev. D **16**, 2219 (1977).
[49] K. Hagiwara, K.-I. Hikasa, and N. Kai, Phys. Rev. Lett. **52**, 1076 (1984).
[50] V. D. Barger, K.-M. Cheung, A. Djouadi, B. A. Kniehl, and P. M. Zerwas, Phys. Rev. D **49**, 79 (1994).
[51] J. M. Butterworth, A. R. Davison, M. Rubin, and G. P. Salam, Phys. Rev. Lett. **100**, 242001 (2008).
[52] D. E. Soper and M. Spannowsky, J. High Energy Phys. 08 (2010) 029.
[53] D. E. Soper and M. Spannowsky, Phys. Rev. D **84**, 074002 (2011).
[54] I. Anderson *et al.*, Phys. Rev. D **89**, 035007 (2014).
[55] C. Grojean, M. Montull, and M. Riembau, J. High Energy Phys. 03 (2019) 020.
[56] A. S. Dighe, I. Dunietz, and R. Fleischer, Eur. Phys. J. C **6**, 647 (1999).

[57] F. James *Statistical Methods in Experimental Physics* (World Scientific, Singapore, 2006).
[58] F. Beaujean, M. Chrzaszcz, N. Serra, and D. van Dyk, Phys. Rev. D **91**, 114012 (2015).
[59] A. Alloul, N. D. Christensen, C. Degrande, C. Duhr, and B. Fuks, Comput. Phys. Commun. **185**, 2250 (2014).
[60] C. Degrande, C. Duhr, B. Fuks, D. Grellscheid, O. Mattelaer, and T. Reiter, Comput. Phys. Commun. **183**, 1201 (2012).
[61] J. Alwall, R. Frederix, S. Frixione, V. Hirschi, F. Maltoni, O. Mattelaer, H. S. Shao, T. Stelzer, P. Torrielli, and M. Zaro, J. High Energy Phys. 07 (2014) 079.
[62] S. Frixione, E. Laenen, P. Motylinski, and B. R. Webber, J. High Energy Phys. 04 (2007) 081.
[63] P. Artoisenet, R. Frederix, O. Mattelaer, and R. Rietkerk, J. High Energy Phys. 03 (**2013**) 015.
[64] T. Sjostrand, L. Lonnblad, and S. Mrenna, arXiv:hep-ph/0108264.
[65] T. Sjöstrand, S. Ask, J. R. Christiansen, R. Corke, N. Desai, P. Ilten, S. Mrenna, S. Prestel, C. O. Rasmussen, and P. Z. Skands, Comput. Phys. Commun. **191**, 159 (2015).
[66] M. L. Mangano, M. Moretti, F. Piccinini, and M. Treccani, J. High Energy Phys. 01 (2007) 013.
[67] A. Greljo, G. Isidori, J. M. Lindert, D. Marzocca, and H. Zhang, Eur. Phys. J. C **77**, 838 (2017).
[68] L. Altenkamp, S. Dittmaier, R. V. Harlander, H. Rzehak, and T. J. E. Zirke, J. High Energy Phys. 02 (2013) 078.
[69] J. M. Campbell and R. K. Ellis, Phys. Rev. D **65**, 113007 (2002).
[70] S. Alioli, F. Caola, G. Luisoni, and R. Röntsch, Phys. Rev. D **95**, 034042 (2017).
[71] F. Campanario, C. Englert, S. Kallweit, M. Spannowsky, and D. Zeppenfeld, J. High Energy Phys. 07 (2010) 076.
[72] Y. L. Dokshitzer, G. D. Leder, S. Moretti, and B. R. Webber, J. High Energy Phys. 08 (1997) 001.
[73] M. Wobisch and T. Wengler, in *Monte Carlo generators for HERA physics. Proceedings, Workshop, Hamburg, Germany, 1998-1999* (DESY, Hamburg, 1998), pp. 270–279, arXiv:hep-ph/9907280.
[74] M. Cacciari, G. P. Salam, and G. Soyez, Eur. Phys. J. C **72**, 1896 (2012).
[75] A. Hoecker *et al.*, arXiv:physics/0703039.
[76] D. Ciupke (2012), http://www.desy.de/f/students/2012/reports/david_ciupke.pdf.gz.